THE TOPOLOGY OF BACKGROUND MAGNETIC FIELDS AND SOLAR FLARE ACTIVITY

A.V. MORDVINOV[1], I.I. SALAKHUTDINOVA[1], L. A. PLYUSNINA[1], N.G. MAKARENKO[2] and L.M. KARIMOVA[2]
[1]*Institute for Solar-Terrestrial Physics, P.O. Box 4026, Irkutsk, 664033, Russia (e-mail: avm@iszf.irk.ru)*
[2]*Institute of Mathematics, 125 Pushkin Street, Almaty, Kazakhstan (e-mail: chaos@math.kz)*

(Received 28 February 2002; accepted 24 July 2002)

Abstract. We investigate the topological properties and evolution of background magnetic fields on synoptic maps from Wilcox Solar Observatory using mathematical morphology methods in terms of the Minkowski functionals. The total length of the neutral line, the total areas occupied by positive and negative polarities, and the Euler characteristics of background magnetic fields vary over an eleven-year cycle. Changes in the length of the neutral line that separates the polarities of the background magnetic field correlate well with flare activity. A time–longitude analysis of solar flare activity revealed a complicated organization and rotation of the entire flare ensemble. On the time–longitude diagram, flare activity is organized into the patterns which follow the rearrangements in background magnetic field and exhibit coexisting and alternating modes of rigid rotation. The character of rotation of the entire flare ensemble is similar to the rotation of background magnetic fields. The emergence of background magnetic fields and changes in their topology and rotation are often accompanied by enhancements in flare activity. A comparative analysis of the topological changes in background magnetic fields and flare activity reveals their causal relation.

1. Introduction

The activity of magnetic fields in the solar atmosphere depends on their topology (Parker, 1979). The large-scale magnetic field of the Sun controls substantially small-scale activity phenomena and governs the overall development of activity in the course of an 11-yr activity cycle (Makarov *et al.*, 2001). In particular, sequences of flares are sometimes causally related to the occurrence of coronal mass ejections (Dere *et al.*, 1997). These latter phenomena, in turn, result from large-scale instabilities in the coronal magnetic fields which could be accompanied by changes in the background magnetic fields (BMF) of the Sun at the photospheric level.

The apparent behaviour of the BMF is governed mainly by the underlying physical processes which include its generation, transport, and diffusion (Sheeley, De Vore, and Shampine, 1986). The flux-transport mechanism due to the regular meridional flows and supergranular diffusion accounts naturally for coherent patterns in the dynamics of large-scale magnetic fields (Sheeley, Nash, and Wang, 1987). Systematic flux eruptions from subphotospheric layers give rise to the rigidly rotating dominant magnetic patterns if the activity is distributed nonuni-

Solar Physics **211:** 241–253, 2002.

formly. However, the detailed dynamics of the BMF and its relation to other activity phenomena are not completely understood. In particular, Bumba and Hejna (1988) demonstrated that solar flares sometimes follow the BMF rearrangements. Causal relationship between magnetic field evolution and flare appearance is also revealed with the use of high-resolution data (e.g., Liu and Zhang, 2001, and references therein).

Previous studies revealed a hierarchy in magnetic activity of the Sun as well a complicated interrelation between large-scale and small-scale activity phenomena (e.g., Bumba, Garcia, and Klvaňa, 2000; Erofeev, 2001). Sunspot groups tend to cluster into the complexes and activity nests (Gaizauskas *et al.*, 1983; Harvey and Zwaan, 1993). There are also long-lived patterns in distributions of solar flares over the heliographic coordinates known as ‘hot spots’ (Bai, 1988). The major flares tend to occur within these superactive zones with a longitudinal extent up to 90°. Physical criteria for identification of these patterns exhibit interconnected active regions which originate from the same source and rotate with the same rate. The lifetime of an activity complex is about of a year with mean longitudinal extent of about 60° (Bumba, Klvaňa, and Garcia, 2000). Magnetic flux emerges discretely in an activity complex and produces solar flares and coronal mass ejections for several months (Feynman, 1997).

Ruzmaikin (1998, 2000) developed a physical mechanism of the magnetic flux emergence through the convective zone as a threshold-crossing phenomenon and explained the relation between large-scale and local magnetic fields. According this mechanism, large-scale disturbances of the mean magnetic field in the convective zone combined with small-scale magnetic fluctuations produce the regular activity patterns on solar surface if the summary field exceeds the buoyancy threshold. In particular, the $\alpha - \Omega$ dynamo modes with azimuthal wave number of 1 and 2 may produce activity complexes separated by 180 deg in heliographic longitude. Both the threshold-crossing mechanism and the flux-transport model (Sheeley, Nash, and Wang, 1987) explain the magnetic activity behaviour in the Hale cycle.

The distribution of activity phenomena over the heliographic longitude is nonuniform. Both active regions and flares on the Sun tend to be concentrated into longitudinal patterns known as the active longitudes (Bumba and Howard, 1969; Bumba, 1976; Vitinsky, Kopecký, and Kuklin, 1986, and references therein). The active longitudes keep their identity from one 11- yr cycle to another (Bumba, Garcia, and Klvaňa, 2000) and the most stable active longitudes persist for several solar cycles (Vitinsky, Kopecký, and Kuklin, 1986). Jetsu *et al.* (1997) revealed two long-lived flare active longitudes separated by about 180° in heliographic longitude. This suggests a physical reason that maintains activity distribution on the time scale much greater than an 11-yr cycle. There are indirect indications for a relic magnetic field (Mursula, Usoskin, and Kovaltsov, 2000) that was captured by the radiative core of the Sun at the earlier stages of its evolution (Kitchatinov, Jardine, and Cameron, 2001). The relic field may generate persistent mean field disturbances within the convective zone at antipodal longitudes which organize small-scale activity into the active longitudes by analogy with the threshold-crossing mechanism (Ruzmaikin, 1998).

In this paper we study the topological properties and evolution of the BMF using methods of mathematical morphology. We juxtapose the changes in the BMF topology with flare activity to study their interrelations. A comparative analysis of the BMF and flare activity reveals a similar time–longitude behaviour and a causal relation between them.

2. BMF Evolution in Terms of the Minkowski Functionals

Mathematical morphology provides an appropriate tool for investigating the geometry and topology of any pattern (Michielsen and De Raedt, 2000, 2001). Necessary mathematical definitions of Minkowski functionals and algorithms for their computations are given in the Appendix. These functionals have a clear geometrical and topological interpretation: they characterize the areas, perimeters and Euler connectivity of some patterns in the image.

We applied the mathematical morphology (Michielsen and De Raedt, 2000) to a sequence of synoptic maps of the solar magnetic field obtained at Wilcox Solar Observatory of Stanford University from 1976 (Hoeksema and Scherrer, 2001). On the synoptic charts, contour lines map the form and connectivity of magnetic structures averaged over a Carrington rotation. The sequence of the maps describes an averaged dynamics of the BMF with all the restrictions inherent in the synoptic map plotting.

On the synoptic maps, the magnetic fields are presented in a great variety of their forms which drift and transform from rotation to rotation. We applied mathematical morphology to obtain topological characteristics of the BMF. When studying changes in the functionals we find some evidence for a causal relation between the evolution of the BMF and flare activity of the Sun. A similar approach is used in the practice of flare forecasting. An important flare predictor relates the measures of complexity of the neutral line to the flare appearance (Hirman, 1986).

When considering a synoptic map, we can divide it into black-and-white cells relative to some given threshold value. The cross-section of the synoptic map at the zero level corresponds the neutral line topology that describes one of the more important active processes on the Sun and is partly traced by prominences on Hα-maps. These black-and-white maps relative to the zero level of the line-of-sight magnetic field were processed to estimate the Minkowski functionals for activity cycles 20–23. In addition to the morphological functionals, changes in the total magnetic flux between subsequent rotations were analyzed. The absolute value of the magnetic flux growth rate characterizes the emergence of magnetic fields and this is an important predictor of the flare appearance (Heyvaerts, Priest, and Rust, 1977).

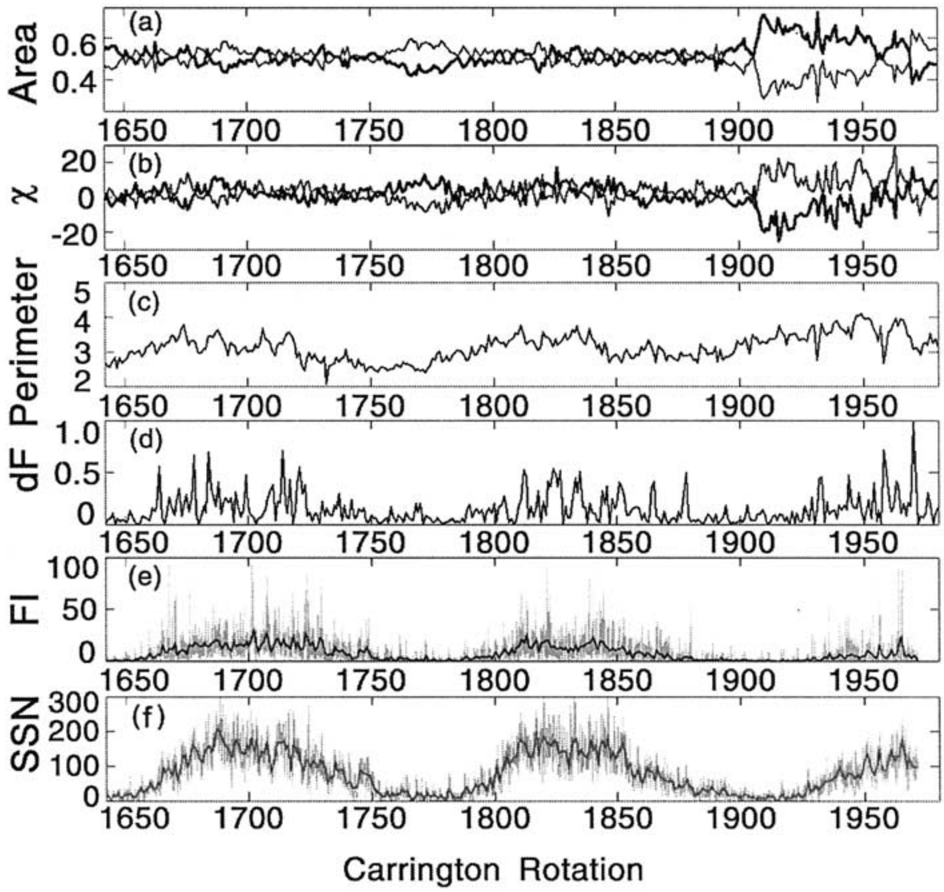

Figure 1. Areas of the positive and negative polarities of the BMF as parts of the whole synoptic map area (a) and their Euler characteristics of BMF (b) shown by the *solid* and *thin curves*, respectively; perimeter is the total length of the neutral line normalized to the length of the edge of synoptic map (c), growth rate of magnetic flux (d), the FI index (e), and the relative sunspot numbers plot (f).

Figure 1a shows the areas of the maps occupied by the positive and negative polarities normalized to the whole area from rotation to rotation. It is remarkable that in the phase of activity rise in cycle 23 during the interval of Carrington rotations 1910–1970 the area of the positive polarity exceeds significantly that for the negative polarity. This leads to a predominance of the positive polarity in the solar mean magnetic field signal and to a monotonic rise of its cumulative sum up to the reversal of the polar magnetic field (Mordvinov and Plyusnina, 2000).

Despite the considerable oscillations in the area and χ during the 1910–1970 period no synchronous flare activity has been observed. This suggests that their small-scale and/or relative changes in the topological characteristics are also important for flare production. Both the polarity asymmetry and the imbalance between the areas reverse at the minima epochs. The cause of the polarity asymmetry is not understood yet, and it is unlikely that it arises due to some technical reason (Grigoryev and Demidov, 1989). Figure 1(b) shows the Euler connectivity χ for both polarities which are estimated using free boundary conditions. Eleven-year cyclic changes are slightly pronounced both in areas and in χ.

Figure 1(c) shows the total length of the contours of the zero line-of-sight magnetic field or the neutral line length. This plot displays well-defined 11-yr cyclic changes. The longer is the neutral line length, the more complicated is the magnetic field topology. Cyclic changes in the perimeter are clearly seen in this figure. At maxima epochs, the BMF grows in size and becomes much more complicated. The internal contours enveloping strong magnetic fields of the active regions contribute also to the measure of BMF complexity.

Figure 1(d) shows the absolute value of the magnetic flux change between consecutive rotations, dF, normalized to its maximum value. Peaks on this plot characterize discrete eruptions of the BMF (Erofeev, 1996). New emerging flux and its interaction with the existing magnetic field is an important condition for the appearance of a flare (Golovko, 1991; Ishkov, 1998). The value of dF quantifies the relation of the BMF to active region magnetic fields, their interaction, and its drastic changes are usually followed by solar flares.

In parallel with a study of topological changes of the BMF, we analyzed flare activity of the Sun as a global process. We studied the time series of the Flare Index (FI) estimated by Ataç and Özgüç (1996, 2001). The FI summarizes daily contributions of solar flares with their power weights and quantifies flare activity of the Sun for 1976–2000 (Ataç and Özgüç, 2000). The faintly visible subflares in Hα images are summarized in daily index FI with a weight coefficient 0.5. This sets a lowest limit on the energy cutoff. Figure 1(e) shows the FI time series and its 27-day running means. This degree of FI smoothing corresponds to the topological data sampling from rotation to rotation and allows us to compare FI with all values from the upper panels.

To study the interrelations between the morphological characteristics, the magnetic flux growth rate, and the FI we estimated the cross-correlations. Linear cross-correlation increases at lags compared with time scales of activity cycle. To study possible causal relation between the parameters on smaller time scales we restrict our consideration in the vicinity of zero lag. The cross-correlation between the Euler connectivity and FI does not exceed 0.4 at about zero lag. More significant cross-correlation between the parameters is also shown in Figure 2. The cross-correlation between the neutral line length and the smoothed FI peaks at the value of 0.76. A significant cross-correlation of 0.83 exists between the neutral line length and the relative sunspot numbers (SSN) (Cugnon, 2001). A significant cross-correlation also exists between the magnetic flux growth rate and FI. The values of the cross-correlations are not impressive, but the most interesting fact is that their maxima are somewhat shifted with positive lags. This means that the flare activity is delayed with respect to the topological changes in the BMF. So, the delay of FI relative to the perimeter changes is about eight Carrington rotations or 218 days.

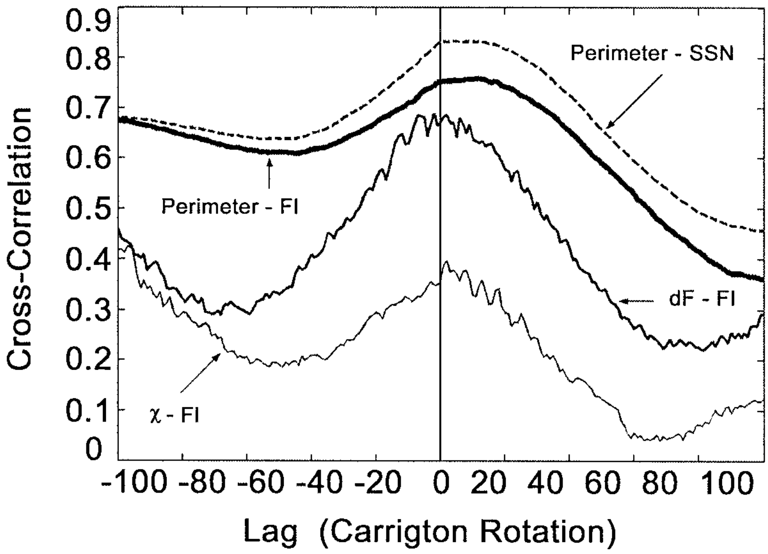

Figure 2. Cross-correlations between the neutral line length, the magnetic flux growth rate, the Euler characteristic, smoothed sunspot numbers, and smoothed FI.

This delay is close to the time which takes an activity complex to develop and to produce flares (Bumba, Klvaňa, and Garcia, 2000).

3. Time–Longitude Analysis of the Flare Activity of the Sun

Although an individual flare is a short-living event, there are long-term patterns in its spatial organization (Altyntsev *et al.*, 1982). Therefore, we can also study the rotation of the whole flare ensemble (Bai, 1988). Patterns in flare activity exhibit a complicated organization and multi-periodic rotation (Bai, 1988; Jetsu *et al.*, 1997; Ataç and Özgüç, 2001).

In this paper we applied the wavelet deconvolution technique (Mordvinov and Plyusnina, 2001) to study the distribution of solar flares in the heliographic longitude based on analyzing the fine structure in the FI signal. The central idea behind the wavelet deconvolution technique is to filter out the component of the FI signal caused by the rotational modulation due to nonuniform flare distribution over heliographic longitude and then to plot this component, rotation by rotation, as a time-longitude diagram. A similar diagram plotted for the solar mean magnetic field revealed multiple modes in solar rotation and their cyclic behavior (Mordvinov and Plyusnina, 2000, 2001). In this study we used the orthogonal Daubechies wavelets as analyzing functions, which have the property of attractive time-scale localization. The discrete wavelet decomposition of FI as a time dependent function on a dyadic time scale may be written as

$$\mathrm{FI}(t) = \sum_{j,k=-\infty}^{\infty} c_{jk}\psi_{jk}(t), \tag{1}$$

where ψ_{jk} are the orthogonal Daubechies wavelets, and the wavelet coefficients determined as the inner products $c_{jk} = \langle \mathrm{FI}\cdot\psi_{jk}\rangle$ (Daubechies, 1992). The essential effects of the rotational modulation fall within the range of timescales from 13 to 30 days. Therefore, when computing the inverse wavelet transform we keep the coefficients which correspond to 8, 16, 32 day time scales. Hence, the filtered component that contains essential rotational effects has the form

$$\delta\mathrm{FI}(t) = \sum_{j=3}^{5} \sum_{k=-\infty}^{\infty} c_{jk}\psi_{jk}(t), \tag{2}$$

with the index j referred to the rotational time scales of 2^j days, where $j = 3,4,5$.

Figure 3(a) shows again the FI for 1976–2000. Using the orthogonal wavelet decomposition over the Daubechies wavelets (Daubechies, 1992) we filtered out the component of the FI signal that contains its rotational modulation on time scales of 8–32 days. This component originates mainly from the rotation of the Sun and due to the non-uniform longitudinal distribution of solar flares, and is shown in Figure 3(b).

Next, we plot the filtered component as a time–longitude diagram with the Carrington rotation folding using the spline interpolation between the daily values. The smoothed diagram of the filtered component is shown in Figure 3(c). This diagram presents a robust distribution of the flare appearance over heliographic longitude. The maximum visibility at the central meridian localizes long-living patterns in heliographic longitude, whereas the influence of short-living events and data inaccuracies are rejected due to the band-pass filtering. At maxima epochs we can see intervals of heliographic longitudes shown in light halftones which display locations of enhanced flare activity. Then we normalized the distribution in Figure 3c to its maximum values for every Carrington rotation (Mordvinov and Plyusnina, 2001) to study the effects of rotation of flare patterns in a compatible form over the 11-yr cycle regardless of the power of events.

The time–longitude distribution of the normalized filtered component is shown twice in Figure 3(d) for a better illustration of the patterns near the edges of the interval 0° or 360°. These diagrams illustrate the relative values of the flare activity within every separate rotation. The location of the hot spots are shown as bright features on the diagrams. These features are arranged as inclined patterns, which indicate the multi-mode rotation of large-scale magnetic fields related to the flare ensemble. The horizontal features appear episodically and exhibit the Carrington

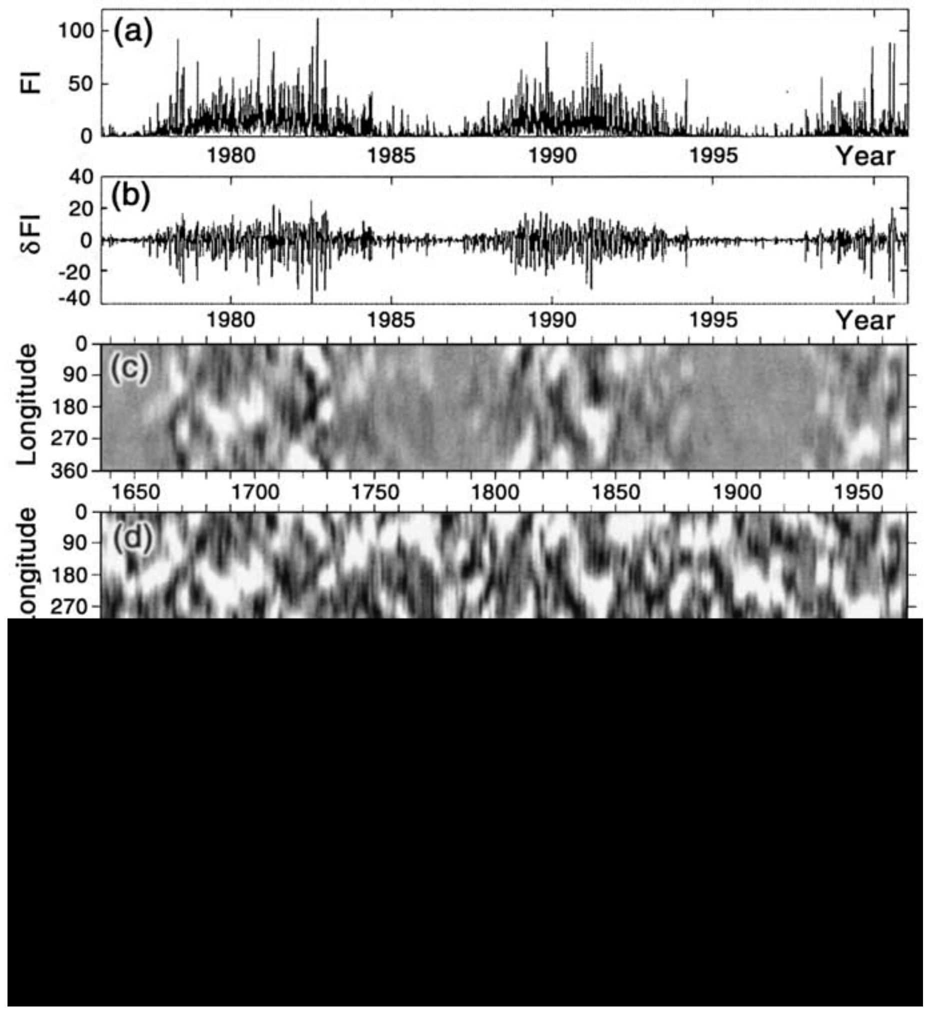

Figure 3. Flare index (a), its rotational modulation component (b), and time–longitude diagram of the filtered component (c), double diagram for normalized FI is compared with the neutral line configuration (*in the middle*) and polarity distribution (*bottom*) of the SMMF signal (d). The letters α and γ mark the BMF emergences which change the rotation mode and the intersections of the rotational modes, respectively.

rotation rate with a period $P = 27.2753$ days. The linear features arranged in a slash '/' direction demonstrate rigid rotation with greater periods of up to 30 days, whereas the features arranged in a back-slash direction '\' correspond to periods shorter than the Carrington period. These rigidly rotating modes coexist and transform one into another by analogy with the discrete rigid modes in BMF rotation (Mordvinov and Plyusnina, 2000).

Figure 3(d) consists of three parts. The upper and the middle parts display twice the normalized time–longitudinal diagram of the δFI component in halftones. The

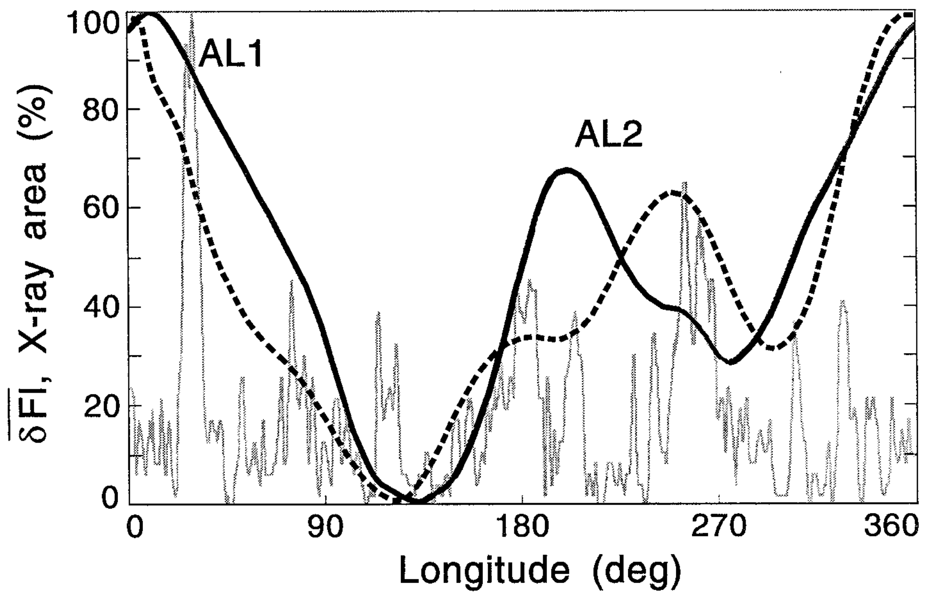

Figure 4. Averaged longitudinal distribution of flare activity over the FI record 1976–2000 obtained through wavelet-deconvolution (*solid*) and the same one for the 1991–2000 period (*dashed*). The distribution of the areas of bright features of X-ray flares averaged over 1991–2001 (*thin*).

lower part displays the time–longitude diagram for the denoised distribution of polarity in the solar mean magnetic field (SMMF) signal that was measured at Wilcox Solar Observatory. The vertical cross-section of the SMMF diagram characterizes the BMF distribution within a given Carrington rotation. The dominant positive polarity is shown in white whereas the negative polarity appears black. The boundary between the dominant polarities is an analog of the neutral line of the large-scale magnetic field. This magnetic separator is mapped in an average sense. The neutral line from this distribution is also superimposed on the δFI diagram in the middle part of Figure 3(d) to compare the time-longitude behaviour of the flare activity and the BMF, which contribute largely to the SMMF signal.

In the middle part of the Figure 3(d), there are some features in the δFI and SMMF diagrams which are arranged in similar inclined patterns. A comparative analysis reveals similarity in both distributions and their causal relation. The events marked by α are characterized by increased flare activity when a new BMF emerges and a new mode of rigid rotation appears. Bumba (1976) found that solar activity strengthens when two rotational modes of BMF intersect. We can see similar intersections of the rotational modes in both distributions. The most evident crossings are marked by γ, and solar activity increases there. All the events and the hot spots with enhanced flare activity are near the neutral line.

The distribution of flare activity slightly varies from cycle to cycle. This is supported by the finding that flares were concentrated at longitudes of about 12°

and 199° over cycles 21 and 22 . When averaging all the distribution shown in Figure 3(c) over the entire record, maxima in flare occurrence take place within the longitudinal intervals 186°–215° and 314°–64°. The averaged distribution shows two flare active longitudes AL1 and AL2 in Figure 4.

To verify the active longitude positions we estimated the longitudinal distribution of the area of bright features of X-ray flares from synoptic maps obtained from the SXT *Yohkoh* observations (http://www.lmsal.com/SXT, 2001) for Carrington rotations 1846–1975. This distribution is plotted as a thin curve in Figure 4. Both plots characterize different flare classes in incompartible scales and their time averaging overlap only in part. Nevertheless, we can see that X-ray flare occurrence peaks near AL1 at 30° longitude. The AL2 is composed of several peaks centered at 183, 204, 252, and 260° heliographic longitudes which dominate at different phases of cycles 21 and 22. When averaging over a wider time interval and taking into consideration the smaller flares, the sharp peaks in flare distribution are dilated and overlap to form AL2. To ease comparison of the X-ray flare distribution with that derived from the wavelet deconvolution technique we also plot the latter averaged for 1991–2000. In Figure 4 these curves also display some common details in flare distributions although the AL2 is somewhat changed in its position and amplitude.

4. Conclusions

Physical information about the BMF can be derived from the topology of their contours and can be described in terms of the topological functionals, whose time dependence facilitates our understanding of solar activity. A significant correlation exists between the BMF topology and the flare activity as a global process. The flare activity delays by about 218 days as compared to the changes in total length of the neutral line of the BMF.

Flare activity of the Sun is arranged in superactive zones and tends to be concentrated within the active longitudes. These patterns of excessive flare activity are characterized by multi-periodic rigid rotation. The rotation of these hot spots is strongly coupled to the BMF eruptions, their evolution and rotation. There is a similar behaviour and a close physical connection between the entire flare ensemble and BMF. Thus, the flare activity reveals its complicated synergy governed by the BMF. Hence, we can conclude that the flare activity is related to BMF dynamics and both phenomena are rooted in subphotospheric layers with the same internal rotation.

Flare activity strengthens when a new portion of the BMF emerges, this phenomena could be accompanied by an appearance of a new mode of rigid rotation of the BMF. The interactions between the rotational modes lead also to enhancements in flare activity during time intervals of the intersection of the modes on the time–longitude diagram. In an averaged sense, flare activity tends to be concentrated within the active longitudes, regardless of its complicated time–longitude organization and its multi-periodic rotation. The entire flare ensemble exhibits active longitudes centered at about 355–12° and 200–245° in the Carrington system. This suggests the presence of global-scale mean field disturbances which persist from cycle to cycle and related possibly to the relic magnetic field of the Sun.

Acknowledgements

The data used in this study were received from the web-sites of the Wilcox Solar Observatory, Sunspot Index Data Center, and the Kandilli Observatory courtesy of Drs J. T. Hoeksema, P. H. Scherrer, P. Cugnon, T. Ataç, and A. Ozguç. The soft X-ray synoptic maps were received from the website of SXT/*Yohkoh* project. We also thank Drs A. A. Golovko, S. A. Yazev, and V. N. Ishkov for useful comments. Special thanks are due to the referee for suggestions which improved the manuscript and Mr V. G. Mikhalkovsky for his assistance in preparing the English version of the manuscript. This work was supported by the RFBR, projects 02-02-16044, 00-15-96659 and INTAS-2001-0550.

Appendix

Mathematical morphology employs additive image functionals to assign numbers to the shape and connectivity of patterns. Integral geometry states (Hadwiger, 1957) that under certain conditions, the number of different additive image functionals is equal to the dimension of the pattern plus one. Thus, in the case of a 2D image there are exactly three of these functionals, called the Minkowski functionals.

An important role in integral geometry belongs to convex bodies. A compact set K in the d-dimensional Euclidean space R^d is called the *convex set* if for every pair of points from K, the entire line segment joining them lies also in K. A convex set with the nonempty interior is called a *convex body*. A single point $x \in R^d$ is also a convex set and a convex body.

Another important notion is the *parallel set*. Let $K \in R^2$ be a compact convex body. Consider the convex body K_ε that is 'parallel' to K, at a distance ε: $K_\varepsilon \subset \bigcup_{i=1}^{N} B_\varepsilon(x_i)$ where $x_i \in K$ and $B_\varepsilon(x_i)$ is a disk, given by

$$B_\varepsilon(x_i) = \{x \in R^2 | \parallel x - x_i \parallel \leq \varepsilon\}.$$

The Steiner formula (Hadwiger, 1957; Mecke and Wagner, 1991) for convex bodies gives a general expression for the 'parallel' volume in R^d:

$$V_\varepsilon(K) = \sum_{i=0}^{d} \binom{d}{i} W_i(K)\varepsilon^i, \tag{3}$$

where $W_i(K)$ are the so-called *Minkowski functionals* (Serra, 1982; Hadwiger, 1957; Mecke and Wagner, 1991; Adler, 1981). Thus, the usual Euclidean measures, namely, the area and volume, of the parallel body can be exactly represented by polynomials of ε. For $d = 2$, there are only three Minkowski functionals. In this case W_0 is the area of the K body, $2\pi W_1$ is the perimeter, and $W_2 = \chi/\pi$. Here, the value of χ is the Euler characteristic of a body. It can be shown that the Minkowski functionals (Adler, 1981) satisfy the following *morphological* properties: *additivity, motion invariance and continuity*. Moreover, $d+1$ Minkowski functionals form a complete system of additive functionals on the set of objects that are unions of a finite number of convex bodies (Hadwiger, 1957).

The functional characterizing the connectivity W_2 in a two-dimensional space, i.e., the Euler characteristic χ, can be introduced other ways (Serra, 1982; Adler, 1981), in particular, as

$$\chi(A \bigcup B) = \chi(A) + \chi(B) - \chi(A \bigcap B) \tag{4}$$

with

$$\begin{array}{ll} \chi(A) = 1 & \text{for convex } A \neq \emptyset, \\ \chi(A) = 0 & \text{for } A = \emptyset. \end{array}$$

It is clear that the black-and-white picture is not always a convex set or a body. However, using the additivity of Minkowski functionals, one can compute them by dividing the image into convex parts (Winitzki and Kosowsky, 1998; Michelsen and De Raedt, 2001). Practical approaches for estimation of the functionals can be found in several papers (Adler, 1981; Serra, 1982; Michelsen and De Raedt, 2001). A matter of some difficulty of the functional's computation consists of taking into account boundary conditions of the image (Winitzki and Kosowsky, 1998; Michelsen and De Raedt, 2001). In this paper we use free boundary conditions.

References

Adler, R. J.: 1981, *The Geometry of Random Fields*. Wiley and Sons, New York.

Altyntsev, A. T., Banin, V. G., Kuklin, G. V., and Tomozov, V. M.: 1982, *Solar Flares*, Moscow, Nauka, p. 247.

Ataç, T. and Özgüç, A.: 1996, *Solar Phys.* **166**, 201.

Ataç, T. and Özgüç, A.: 2000, available in http://www.koeri.boun.edu.tr

Ataç, T. and Özgüç, A.: 2001, *Solar Phys.* **198**, 399.

Bai, T.: 1988, *Astrophys. J.* **328**, 860.

Bumba, V.: 1976, in V. Bumba and J. Kleczek (eds.), *Basic Mechanisms of Solar Activity,* D. Reidel Publ. Co, Dordrecht, Holland, p. 47.

Bumba, V. and Hejna, L.: 1988, *Bull. Astron. Inst. Czech.* **39**, 8.

Bumba, V. and Howard, R.: 1969, *Solar Phys.* **7**, 28.

Bumba, V., Garcia, A., and Klvaňa, M.: 2000, *Solar Phys.* **196**, 403.

Bumba, V., Klvaňa, M., and Garcia, A.: 2000, in A. Wilson (ed), *The Solar Cycle and Terrestrial Climate*, ESA, ESTEC, Noordwijk, The Netherlands, p. 289.

Cugnon, P.: 2001, available in http://sidc.oma.be

Daubechies, I.: 1992, *Ten Lectures on Wavelets*, Society for Industrial and Applied Mathematics. Philadelphia.
Dere, K. P. and 33 co-authors: 1997, *Solar Phys.* **175**, 601.
Erofeev, D. V.: 1996, *Solar Phys.* **167**, 25.
Erofeev, D. V.: 2001, *Solar Phys.* **198**, 31.
Feynman, J.: 1997, in N. Crooker, J. A. Joselin, and J. Feynman (eds.), *Coronal Mass Ejections*, Geophys. Monograph 99, AGU, p. 49.
Gaizauskas, V., Harvey, K. L., Harvey, J. W., and Zwaan, C.: 1983, *Astrophys. J.* **265**, 1056.
Golovko, A. A.: 1991, *Issledovaniya po geomagnetizmu, aeronomii i fizike Solntsa* **95**, Irkutsk, Russia, p. 172.
Grigoryev, V. M. and Demidov, M. L.: 1989, *Solar Magnetic Fields and Corona*, Novosibirsk, Russia, p. 108.
Hadwiger, H.: 1957, *Vorlesungen uber Inhalt, Oberflache und Isoperimetric*. Springer-Verlag, Berlin.
Harvey, K. L. and Zwaan, C.: 2000, *Solar Phys.* **197**, 1.
Heyvaerts, J., Priest, E. R., and Rust, D. M.: 1977, *Astrophys. J.* **216**, 123.
Hirman, J. V.: 1986, in P. A. Simon, G. Heckman and M. A. Shea (eds), *Solar-Terrestrial Predictions*, NOAA Boulder, p. 384.
Hoeksema, J. T. and Scherrer, P. H.: 2001, available in http://quake.stanford.edu
Ishkov, V. N.: 1998, *Izvestiya of the Russian Academy of Sciences, Ser. Phys.* **62**, 1835.
Jetsu, L., Pohjolainen, S., Pelt, J., and Tuominen, I.: 1997, *Astron. Astrophys.* **318**, 293.
Kitchatinov, L. L., Jardine, M., and Cameron, A. C.: 2001, *Astron. Astrophys.* **374**, 250.
Liu, Y. and Zhang, H.: 2001, *Astron. Astrophys.* **372**, 1019.
Makarov, V. I., Tlatov, A. G., Callebaut, D. K., Obridko, V. N., and Shelting, B. D.: 2001, *Solar Phys.* **198**, 409.
Mecke, K. R. and Wagner, H.: 1991, *J. Statist. Phys.* **64**, 843.
Michielsen, K. and De Raedt, H.: 2000, *Comp. Phys. Commun.* **132**, 94.
Michelsen, K. and De Raedt, H.: 2001, *Phys. Rep.* **347**, 461.
Mordvinov, A. V. and Plyusnina, L. A.: 2000, *Solar Phys.* **197**, 1.
Mordvinov, A. V. and Plyusnina, L. A.: 2001, *Astron. Rep.* **45**, 652.
Mursula, K, Usoskin, I. G., and Kovaltsov, G. A.: 2000, in A. Wilson (ed), *The Solar Cycle and Terrestrial Climate*, ESA, ESTEC, Noordwijk, The Netherlands, p. 387.
Parker, E. N.: 1979, *Cosmical Magnetic Fields*, Oxford University Press, Oxford.
Ruzmaikin, A.: 1998, *Solar Phys.* **181**, 1.
Ruzmaikin, A.: 2000, *Solar Phys.* **192**, 49.
Serra, J.: 1982, *Image Analysis and Mathematical Morphology*, Vol. 1, Academic Press, London.
Sheeley, N. R. Jr., De Vore, C. R., and Shampine, L. R.: 1986, *Solar Phys.* **106**, 251.
Sheeley, N. R., Nash, A. G., and Wang Y. M.: 1987, *Astrophys. J.* **319**, 481.
SXT/*Yohkoh* project, available in http://www.lmsal.com/SXT/
Vitinsky, Yu. I., Kopecký, M. and Kuklin, G. V.: 1986, *Statistics of sunspot activity of the Sun*, Nauka, Moscow (in Russian).
Winitzki, S. and Kosowsky, A.: 1998, *New Astron.* **3**, 75.